# Phononic Crystals: Physical Principles and Novel Structures

**Amir Rostami[1], Hassan Kaatuzian[1*], Babak Rostami-Dogolsara[2]**

[1]Photonics Research Laboratory, Electrical Engineering Department,

Amirkabir University of Technology (Tehran Polytechnic), Tehran, Iran

[2]Department of Electrical Engineering, Lahijan branch, Islamic Azad University, Lahijan, Iran

[*]**Corresponding author: Hassan Kaatuzian, PhD, Professor,** Email: hsnkato@aut.ac.ir

## Abstract

Phononic crystals (PnCs) are periodic materials that can control and manipulate the propagation of acoustic (or elastic) waves. The importance of paying attention to this area can be seen in applications such as wireless telecommunications, communication systems in shallow water, sensors, acoustic signal processing, and ultrasonic imaging. During the last two decades, various devices have been proposed, fabricated, and measured and a great amount of research has implemented topology optimization for designing these structural materials as well as the associated functional devices. In this study, a comprehensive overview of the state-of-the-art advances in governing principles of PnC operations are discussed, including the study of the background of PnCs, their types and topologies, their applications in different fields, as well as their filtering and guiding properties. In this paper, we've reviewed two of our own work. First, a 1x2 multiplexer which is designed from two ring resonators and estimated Quality(Q) factor and frequency channel crosstalk at different temperatures(10<T<40℃) and pressures(0.1<P<5MPa). Second, an acoustic channel drop filter and evaluation of Q-factor with changes in parameters such as pressure, temperature and molality (0.9<M<0.1 mol/Kg). In addition to our works, some of other proposed simulated or fabricated structures are also presented. The relations and computational methods for solving the equations used in these structures are investigated which is the Finite Difference Time Domain (FDTD) method.

**Keywords:** phononic crystal, acoustic waveguide, defect, filter, demultiplexer

## 1 INTRODUCTION

Investigation of acoustic waves in phononic crystals (PnC) which are the periodic structures has always been considered due to their unique features. They are composed of a periodic arrangement of two different types of materials in which the propagation of acoustic/elastic waves is completely forbidden[1-9]. The destructive interference of the scattered waves by the rods (inclusions) of the PnC is the general mechanism for the opening of a phononic band-gap. On the other hand, the main property of PnCs is that at a certain range of frequencies, they do not allow mechanical waves (acoustic or elastic) to propagate inside the structure. According to the size of inclusions, the filling factor, the topology, and the lattice constant of the PnC, mechanical waves to be reflected in a certain range of frequencies and not to be propagated in the lattice. As a result, it can be used to control and manipulate mechanical waves with the desired frequency. Stated otherwise, Bloch waves become evanescent inside band gaps[10-17].

It should be noted that the position and width of the various types of bandgaps depend on the direction of motion of the acoustic wave inside the crystal[18]. Such gaps may take place for specific directions of the wave vector. In other words, the formation of wide acoustic bandgap depends on two factors. (1) The existence of high contrast between the elastic properties of the materials should be required. (2) The filling factor of the inclusions should be sufficient. The PnCs are used to tune the acoustic/elastic waves[19-29], which have many important properties, such as band gaps[30-41], band-edge states[42-49], and having the ability of slow-wave effect[50-55].

In terms of dimensions, the PnCs are divided into three categories. The first is one-dimensional systems (superlattices, comb-like structures, or Bragg lattices)[56-63] that allow longitudinal, transverse, and mixed modes. The second is two-dimensional systems which are the arrays of infinitely long rods embedded in the background matrix[64-69]. The third is three-dimensional systems[40,70-75] (spherical inclusions that are suspended in a host matrix) in which the longitudinal and transverse modes are strongly coupled, complicating the nature of the eigenmodes and the corresponding computations. The transverse and longitudinal waves are decoupled in a homogeneous bulk medium which are propagated independently. In a longitudinal wave, the displacement vector field $\boldsymbol{u}$ is potential ($\nabla \times \boldsymbol{u}=0$), while, it is solenoidal ($\nabla . \boldsymbol{u}=0$) in a transverse wave. The continuity of the displacements and stresses causes to mixing of these two modes in the presence of a boundary[76-78]. The different types of the PnC based on dimensions are shown in Fig. 1(a), similar to[79]. The different colors in this Fig. represent materials with different properties. An example of a band structure is shown in Fig. 1(b). Since the band structure is also small compared to the dimension of the structure (the band gap can be tuned to any mechanical wavelength), many macroscopic structures from the frequency range of sonic (kHz)[80-82], to ultrasonic (MHz)[83-85] would be studied. Nowadays, there is a great interest in band structure in new structures and materials, fabrication technology of sub-micron structures, and working in hypersonic regimes (GHz)[86-88], as well as heat control (THz)[89-91], which are shown in Fig. 1(c). It should be noted that phonons can be excited electrically in the frequency range of GHz. They are used in sensing and imaging applications as well as Micro or Nanoelectromechanical systems, known as MEMS/NEMS. The sources of phonons in the very-high-frequency range are the thermal vibrations of atoms or molecules which are called thermal phonons.

In this reviewal study, in section 2, we'll categorize different types of PnC. Section 3 describes fabrication of PnC. Bulk elastic wave equations in solids and fluids and also dispersion relation, will be discussed in section 4. Effects of defects and guiding in PnC will be explained in sections 5 and 6. Filtering and de-multiplexing will be reviewed in sections 7 and 8. At last we'll have a conclusion section 9.

***a)***

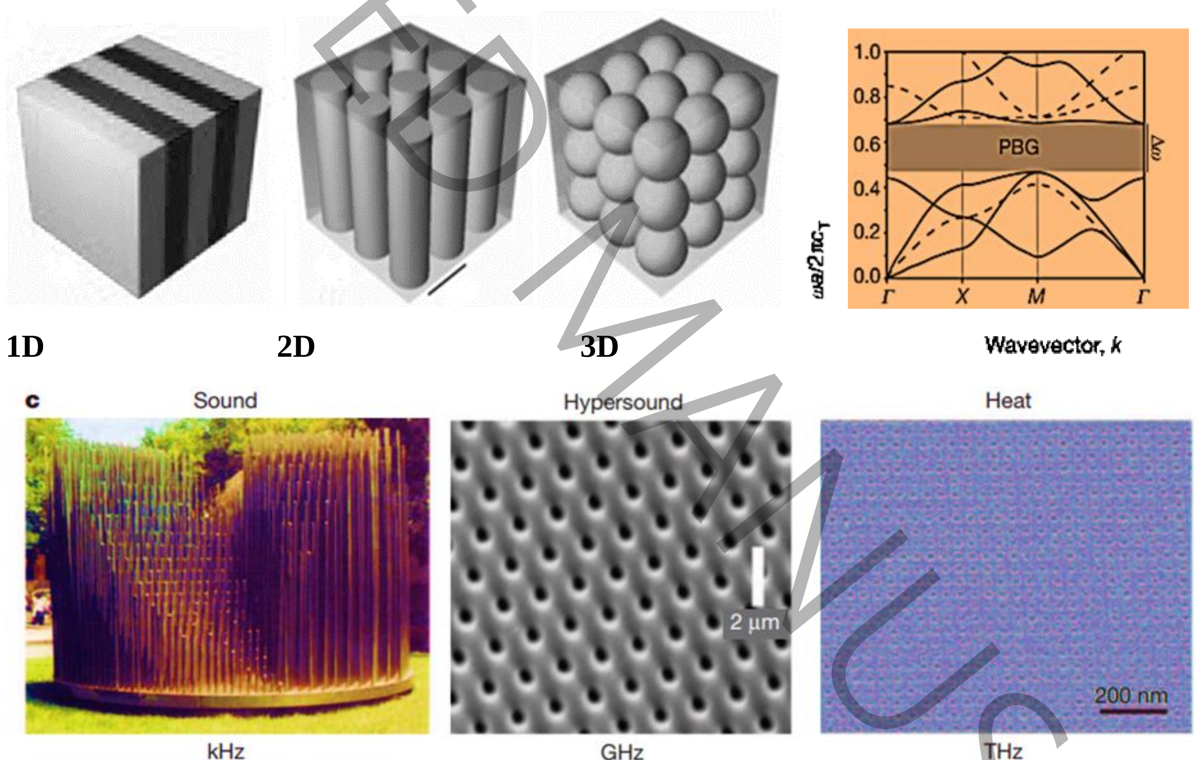


**Fig. 1. Phononic crystals. (a) 1D, 2D and 3D PnC; (b) An example of a phononic band structure; (c) 2D PnCs with periodicities in the range of kHz (sound), GHz (Hypersound), THz (Heat), which are indicated from left to right, respectively, Ref[79].**

## 2 CATEGORIZING DIFFERENT TYPES OF PHONONIC CRYSTALS

In terms of the types or the forms of material, the PnCs are divided into three other categories which are solid-solid[92-96], solid-liquid[97-99], and liquid-liquid[100].

There have also been some PnCs designs that show self-collimation of elastic waves[101,102], PnCs with different properties in different directions[103], PnCs in which they are robust to imperfections[104-106], topology optimization of PnCs[107], piezoelectric PnCs[108], the wave attenuation in viscoelastic materials[109] and maximizing absolute and relative band gaps[110].

The progress in the field of PnCs (or PC) goes in parallel with their photonic crystal (PtC) counterparts. However, the variety of materials in PnCs is much greater than those of PtCs. In this regard, there is the possibility of high contrast among the elastic properties, large acoustic absorption, and the solid or fluid nature of the constituents[78,111]. The electromagnetic equations are as follow[112]:

$$\frac{\partial E_z}{\partial x} = -i\omega\mu_y H_y \quad (1)$$

$$\frac{\partial E_z}{\partial y} = -i\omega\mu_x H_x \quad (2)$$

Where $E$ and $H$ are electric and magnetic field, respectively. The acoustic equations are as follow[112]:

$$\frac{\partial P}{\partial x} = -i\omega\rho_x u_x \quad (3)$$

$$\frac{\partial P}{\partial y} = -i\omega\rho_y u_y \quad (4)$$

$$\frac{\partial u_x}{\partial x} + \frac{\partial u_y}{\partial y} = -i\omega\beta P \quad (5)$$

Where $P$ and $U$ are acoustic pressure and displacement, respectively. The comparison between electromagnetic and acoustic variables is shown in Table 1[112].

**Table 1. Comparison between the electromagnetic and acoustic variables and material properties[112]**

| Acoustic | Electromagnetic | Comparison |
|---|---|---|
| Acoustic Pressure (P) | Electric Field ($E_z$) | $-E_z \leftrightarrow P$ |
| Particle Velocity ($u_x u_y$) | Magnetic Field ($H_x H_y$) | $H_y \leftrightarrow -u_x \quad H_x \leftrightarrow u_y$ |
| Dynamic Density ($\rho_x \rho_y$) | Permeability ($\mu_x \mu_y$) | $\rho_x \leftrightarrow \mu_y \quad \rho_y \leftrightarrow \mu_x$ |
| Dynamic Compressibility ($\beta$) | Permittivity ($\varepsilon_z$) | $\varepsilon_z \leftrightarrow \beta$ |

It should be noted that all the ordinary (electronic) crystals, PtCs, and PnCs with identical lattices give rise to the same Bragg diffractions. However, the characteristics of these mentioned periodic crystals have significant differences which are explained in Table 1[113].

**Table 1 Comparison between the properties of three periodic systems of electronic crystal, PnC and, PtC[113]**

| Property | Electronic Crystal | Photonic Crystal (PtC) | Phononic Crystal (PnC) |
|---|---|---|---|
| Materials | Crystalline (Natural or grown) | Constructed of two dielectric materials | Constructed of two elastic materials |
| Parameters | Universal constants, atomic numbers | Dielectric constants of constituents | Mass densities, sound speeds $C_T$, $C_L$ of constituents |
| Lattice constant | 1-5Å (microscopic) | 0.1µm to 1cm (mesoscopic or macroscopic) | Mesoscopic or macroscopic |
| Waves | de Broglie (electrons) $\psi$ | Electromagnetic or light (photons) $\bar{E}$, $\bar{B}$ | Vibrational or sound (phonons) $\bar{u}$ |
| Polarization | Spin (up, down) | Transverse: $\nabla.\bar{D}=0$ $\nabla\bar{E}\neq 0$ | Coupled Transverse - Longitudinal. $\left(\nabla.\bar{u}\neq 0, \nabla\times\bar{u}\neq 0\right)$ |
| Free particle limit | $W=\dfrac{\hbar^2k^2}{2m}$ (electrons) | $\omega=\dfrac{c}{\sqrt{\epsilon}}k$ (photons) | $\omega=c_{t,l}k$ (phonons) |
| Band-gap | Increases with crystal potential; no electron states | Increases with $\left\|\epsilon_a-\epsilon_b\right\|$ no photons, no light | Increases with $\left\|\rho_a-\rho_b\right\|$ , etc. no vibration, no sound |
| Spectral region | Radio wave, microwave, optical, X-ray | Microwave, optical | $\omega \lesssim 1GHz$ |

## 3 FABRICATION OF PnC

In this section, we will explain the procedure of fabricating a functional device based on PnC slab, which is made by the array of holes in a Si membrane[114]. The conformity of the frequency range of operation of such devices to the frequencies appropriate for sensing applications and wireless communication is vital role in designing and fabricating process. Choosing the suitable thickness of the slab and the appropriate radius of the holes in the square-lattice of PnC are effective parameters in opening the complete phononic band gag (PnBG). In this case, the hole radius is $r$=6.4μm, lattic constant is $a$=15μm, and the thickness of Si layer is $d$=15μm with the frequency range of 119MHz< f <150MHz.

First of all, the silicon on insulator (SOI) is used as substrate and the thickness of the Si layer is 15μm which is shown in Fig. 2(a). In order to form the lower electrode of the transducer, a thin layer of gold (with the thickness of ~100nm) in the lift-off process is evaporated and patterned on the Si layer, shown in Fig. 2(b). In order to add the effect of piezoelectric for exiting the elastic wave, 1μm layer of Zinc oxide (ZnO) is deposited and patterned using sputtering and wet etching, which are shown in Fig. 2(c). To form the second set of electrodes, a layer of aluminum is patterned which is shown in Fig. 2(d). The PnC holes are patterned in Si layer using optical lithography which is followed by deep plasma etching (Fig. 2(e)). In order to form the PnC membrane, the Si substrate and oxide layer are removed by backside lithography which is shown in Fig. 2(f). The top view and the cross-sectional view of scanning electron microscope (SEM) images for a typical fabricated device are shown in Fig. 3.

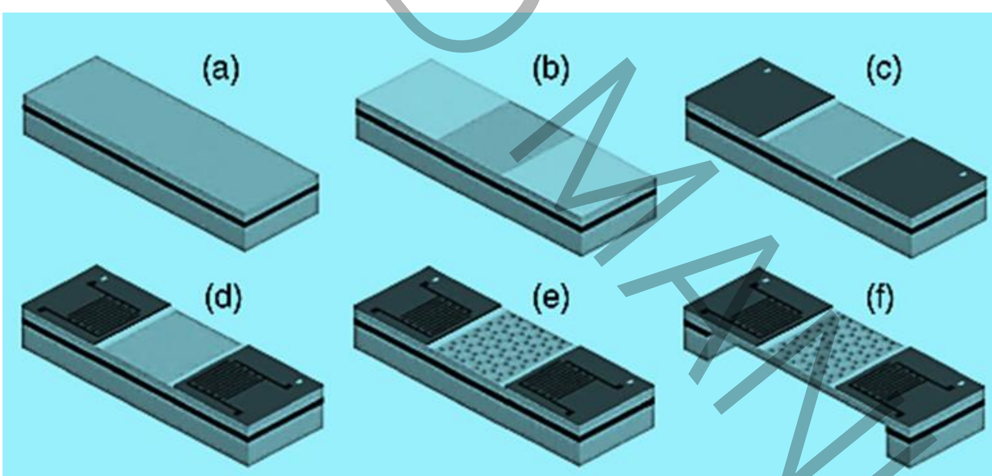


**Fig. 2. Fabrication steps for Si PC plate structures. (a) SOI substrate; (b) deposition of the lower electrode and patterning; (c) sputtering and patterning of ZnO layer; (d) deposition of the top metal electrode and patterning; (e) etching process and creating PnC holes; (f) final structure is achieved by plasma etching of the lower Si substrate, Ref.[114].**

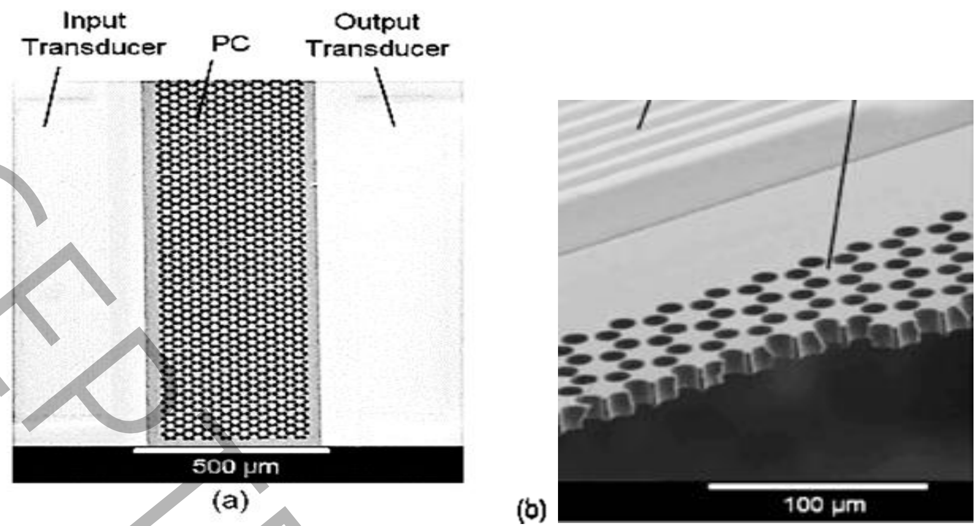


**Fig. 3. Top view (a) and cross-sectional view (b)** of the fabricated devices, Ref.[114].

The lowest anti-symmetric Lamb wave in micro-fabricated piezoelectric phononic plates is investigated. The structure is based on an AT-cut quartz plate which is consisted of a gradient-index phononic crystal (GRIN PC) lens and a linear phononic plate waveguide[115]. Fig. 4 shows the micro-fabrication process of this device. In order to make the sidewall of the holes close to vertical, the upper and lower sides of the quartz plate were etched. On the both sides of the quartz plate the Gold-Chromium (Au/Cr) films were sputtered. The Cr film which is located between the Au film and quartz plate acts as the adhesion layer (Fig. 4(a)). To form the periodic cylinders, the photoresist with the thick of 8μm was patterned on the front-side of the quartz plate (Fig. 4(b)). To prevent the 80μm thick quartz plate from bending and breaking the double-side Au/Cr seed layers and the double-side Nickel (Ni) electrodeposition was used (Fig. 4(c)). Then the photoresist was removed (Fig. 4(d)). The Au/Cr layer was not covered by the Ni mask. So, the Xenon (Xe) gas is used to remove it. The Sulfur hexafluoride (SF6) gas was used to etch (with the etching rate of 450nm/min) the front-side of the quartz plate. To fabricate the vertical sidewall of the cylindrical air hole, the etching process should be divided into two steps. At the first step, the depth of etching of front-side should be 40μm and the Ni mask was removed by using the nitric acid (Fig. 4(e)). In the next step, the back-side of quartz plate was patterned again, followed by Ni electroplating and photoresist removal. By using the same process for the front-side, the back-side of the quartz plate was etched and the selectivity of the Ni mask to quartz plate was 20. Then, the Ni mask was removed by using nitric acid and the PC gratings were accomplished (Fig. 4(f)-(h)). At the end, the interdigital transducers (IDT) were fabricated onto the left-side of the GRIN PC plate lens to generate 10MHz Lamb waves using the photolithography process (Fig. 4(i) and (j)).

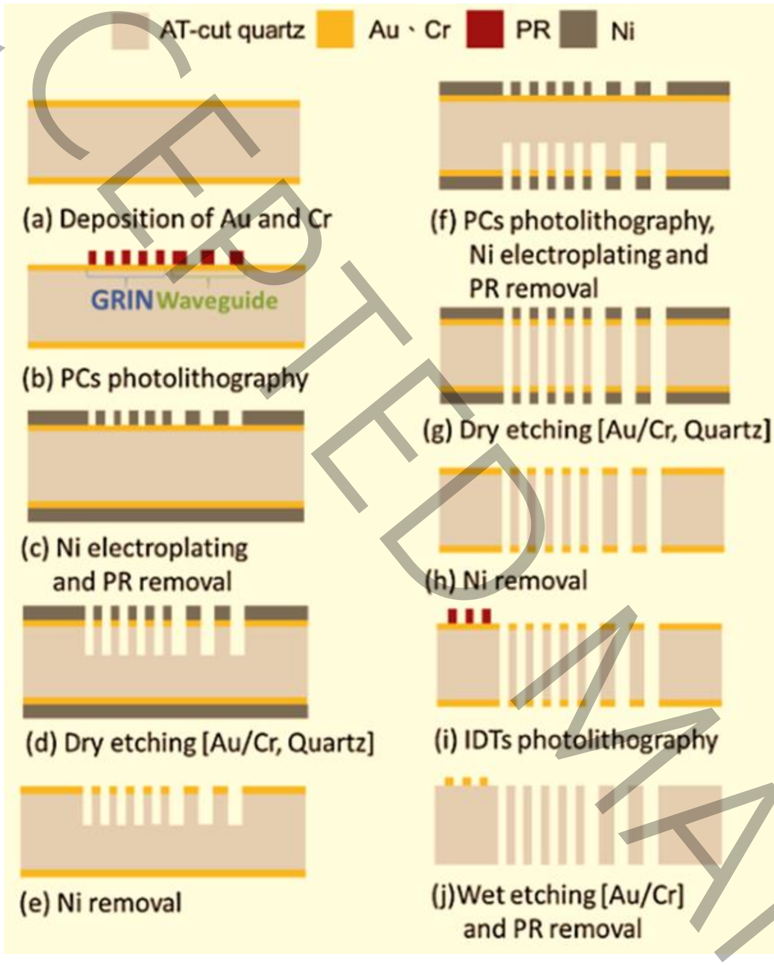


**Fig. 4. The micro-fabrication process of the GRIN PC lens and waveguide, Ref[115].**

## 4 EQUATIONS

### 4.1 The Bulk Elastic Wave in Solid Inhomogeneous Material

In this section, we want to investigate the propagation of elastic waves in solids. Solid materials are made of periodic and precise order of atoms in space. When the plane wave of the elastic wave with the wave vector of $k$ propagates inside the crystal, the collective and coherent movements of atoms take place[116-118]. The displacement of the atom from its equilibrium position is due to a forward perturbation caused by the elastic plane wave and is indicated by the displacement vector of $U(r, t)$[119-121].

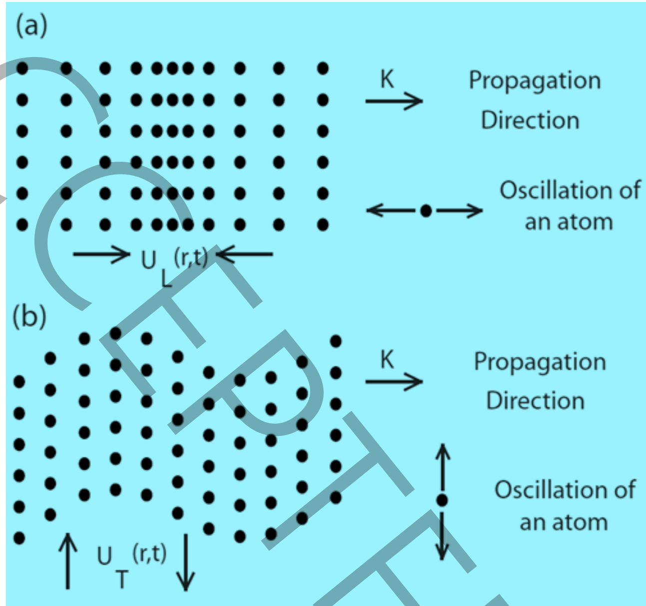


**Fig. 5. The displacement of a square lattice during the propagation of bulk waves: (a) Longitudinal $U_L(r, t)$, and (b) Transverse $U_T(r, t)$, Ref. [121].**

When atoms move perpendicular to the direction of propagation, the displacement vector $U(r, t)$ is perpendicular to the direction of propagation, and the elastic plane wave is called the transverse plane wave (Fig. 5(a)). When atoms move along the direction of propagation, the elastic plane wave is called the longitudinal plane wave (Fig. 5(b)). An important feature of the elastic wave propagation inside the homogeneous solid is that the transverse or longitudinal elastic waves propagate at different speeds and they are independent of each other. In solids, the transverse velocity of the elastic plane wave is denoted by $C_t$, while the longitudinal velocity of elastic plane wave is denoted by $C_l$. The propagation of transverse/longitudinal elastic plane wave with the frequency of $\omega$ in the solid material is denoted by[119,120].

$$U_T(r.t) = \mathrm{Re}\left(u_{T0}\ e^{i(k.r-\omega t)}\right) \tag{6}$$

$$U_L(r.t) = \mathrm{Re}\left(u_{L0}\ e^{i(k.r-\omega t)}\right) \tag{7}$$

where $U_T(r, t)$ and $U_L(r, t)$ are the transverse and longitudinal displacement, respectively. They are also perpendicular and parallel to the wave vector of $k$, respectively. $u_{T0}$ and $u_{L0}$ are the amplitude of the displacement vector. In solid homogeneous material[119,120]

$$\nabla_T^2 u = \frac{1}{C_T^2}\frac{\partial_T^2 u}{\partial t^2}\ . \tag{8}$$

and

$$\nabla_L^2 u = \frac{1}{C_L^2}\frac{\partial_L^2 u}{\partial t^2}\ . \qquad (9)$$

Substitution of Eq.s (6 and (7 into Eq.s (8 and (9 leads to calculating the equations for transverse / longitudinal wave number

$$\boldsymbol{k_T} = \frac{\boldsymbol{\omega}}{\boldsymbol{c_T}} \qquad (10)$$

and

$$\boldsymbol{k_L} = \frac{\boldsymbol{\omega}}{\boldsymbol{c_L}} \qquad (11)$$

$c_T$ and $c_L$ are determined by the mechanical properties of the material and calculated by

$$c_T = \sqrt{\frac{\mu}{\rho}} \qquad (12)$$

and

$$c_L = \sqrt{\frac{\lambda + 2\mu}{\rho}} \qquad (13)$$

where $\rho$ is mass density, $\lambda$ and $\mu$ are the Lame coefficients. The Lame coefficients describe the mechanical properties of solids which are calculated by the following equations

$$\lambda = \frac{E\vartheta}{(1+\vartheta)(1-2\vartheta)} \qquad (14)$$

and

$$\mu = \frac{E}{2(1+\vartheta)} \qquad (15)$$

where $E$ and $\vartheta$ are the Young modulus and Poisson coefficient. ω

**4.2 Acoustic Waves in Fluid Materials**

The important point is that only longitudinal waves propagate in fluid materials. No transverse mods are allowed in any fluid-fluid materials[116,117]. In homogenous fluid-fluid systems, the propagation of acoustic waves expresses in the form of instantaneous pressure $p(r.t)$ which is defined by [78]

$$p(r.t) = -\lambda \nabla . u(r.t) \quad (16)$$

The acoustic wave of instantaneous pressure with the frequency of $\omega$ is calculated by

$$p(r.t) = Re\left(p_0\, e^{i(k.r-\omega t)}\right) \quad (17)$$

Using the above equations, the propagation of acoustic waves in the homogenous fluid materials is calculated by

$$\nabla^2 p = \frac{1}{c_0^2}\frac{\partial^2 p}{\partial t^2} \quad (18)$$

where $c_0$ is the velocity of the acoustic wave. The equation for acoustic wave number is

$$\boldsymbol{k}_0 = \frac{\boldsymbol{\omega}}{\boldsymbol{c}_0} \quad (19)$$

where the $c_0$ is calculated by

$$c_0 = \sqrt{\frac{\lambda}{\rho}} \quad (20)$$

**4.3 Dispersion Relationship**

One of the most common methods for investigating the phononic gaps is the structure of the PnC is assumed to be infinite, filling the entire space with a one-dimensional structure.

Generally, the dispersion relationship of $\omega=\omega(k)$ for the propagation of the elastic wave in the infinite solid-solid PnC structure is calculated by solving the wave equation for heterogeneous solid materials[78]:

$$\nabla \cdot \left(\rho c_T^2 \nabla u_i + \rho c_T^2 \frac{\partial u}{\partial x_i}\right) + \frac{\partial}{\partial x_i}\left(\left(\rho c_L^2 - 2\rho c_T^2\right) \nabla . u\right) = -\rho\left(\omega(k)\right)^2 u_i \quad (21)$$

where $u = u_r(r)$ is displacement vector of the elastic wave inside the PnC structure with the wave vector of $k$.

**4.4 One Dimensional PnC**

In one-dimensional PnCs, the change in material properties is only in one direction. We want to consider the periodic solid layers. The elastic waves propagate perpendicular to the layers with the wave vector of $\boldsymbol{k} = k_x \hat{x}$.

In order to obtain the band structure of the 1D PnC, the Eq. (21 is divided into the following three equations in $x, y$ and $z$ directions[78]:

$$\frac{\partial}{\partial x}\left(\rho c_L^2 \frac{\partial u_x}{\partial x}\right) = -\rho\left(\omega(k)\right)^2 u_x \tag{22}$$

$$\frac{\partial}{\partial x}\left(\rho c_T^2 \frac{\partial u_y}{\partial x}\right) = -\rho\left(\omega(k)\right)^2 u_y \tag{23}$$

$$\frac{\partial}{\partial x}\left(\rho c_T^2 \frac{\partial u_z}{\partial x}\right) = -\rho\left(\omega(k)\right)^2 u_z \tag{24}$$

where $u_x = u_x(x)$ , $u_y = u_y(y)$ and $u_z = u_z(z)$. It should be noted that these three equations are independent of the displacement vector of $u_x$, $u_y$ and $u_z$. It means that the elastic wave can propagate inside the PnC structure independently as either longitudinal elastic wave with $u_x$ or transverse elastic wave with $u_y$ and $u_z$. It should be pointed out that the mentioned PnC structure has periodic layers in the $X$ direction. As a result, it could not prevent the propagation of waves that are parallel to the layers ($X$ and $Y$ direction).

### 4.5 Two-dimensional PnC

In two-dimensional PnCs, the change in material properties is in two directions ($x$, $y$), and there is no changes in $z$ direction. In other words, the parameters of the structure change in the form of $\rho(x.y)$, $c_T(x.y)$ and $c_L(x.y)$. Using Eq. (21, the dispersion curve in two-dimensional structures is obtained as follows[78]:

$$\frac{\partial}{\partial x}\left(\rho c_L^2 \frac{\partial u_x}{\partial x} + \left(\rho c_L^2 - 2\rho c_T^2\right)\frac{\partial u_y}{\partial y}\right) + \frac{\partial}{\partial y}\left(\rho c_T^2 \frac{\partial u_x}{\partial y} + \rho c_T^2 \frac{\partial u_y}{\partial x}\right) = -\rho\left(\omega(k)\right)^2 u_x \tag{25}$$

$$\frac{\partial}{\partial y}\left(\rho c_L^2 \frac{\partial u_y}{\partial y} + \left(\rho c_L^2 - 2\rho c_T^2\right)\frac{\partial u_x}{\partial x}\right) + \frac{\partial}{\partial x}\left(\rho c_T^2 \frac{\partial u_y}{\partial x} + \rho c_T^2 \frac{\partial u_x}{\partial y}\right) = -\rho\left(\omega(k)\right)^2 u_y \tag{26}$$

$$\frac{\partial}{\partial x}\left(\rho c_T^2 \frac{\partial u_z}{\partial x}\right) + \frac{\partial}{\partial y}\left(\rho c_T^2 \frac{\partial u_z}{\partial y}\right) = -\rho\left(\omega(k)\right)^2 u_z \tag{27}$$

These equations show that elastic waves inside the PnC can be propagated in two ways. The Eq.s (25 and (26 show the propagation of coupled elastic waves whose displacement vectors have coupled the components of $u_x$ and $u_y$. These elastic waves are called In-Plane waves. Eq. (21 shows the propagation of independent waves that are specified by the component of displacement vector and are perpendicular to the plane. This elastic wave, which propagates independently and perpendicular to the $k$ wave vector, is called the Out-of-Plane wave.

## 5 THE POINT DEFECT AND LINE DEFECT ON PnCs

Applying point defect and line defect in the structure of PnC makes them possible to use them in devices such as acoustic waveguides and cavities. In other words, the defect modes can be created within the acoustic (elastic) wave band gaps due to the locally breaking the periodicity of the structures[122]. Point defects create straight bands in the phononic gap that causes wave confinement and form cavities. An example of these defects is shown in

Fig. 6[123].

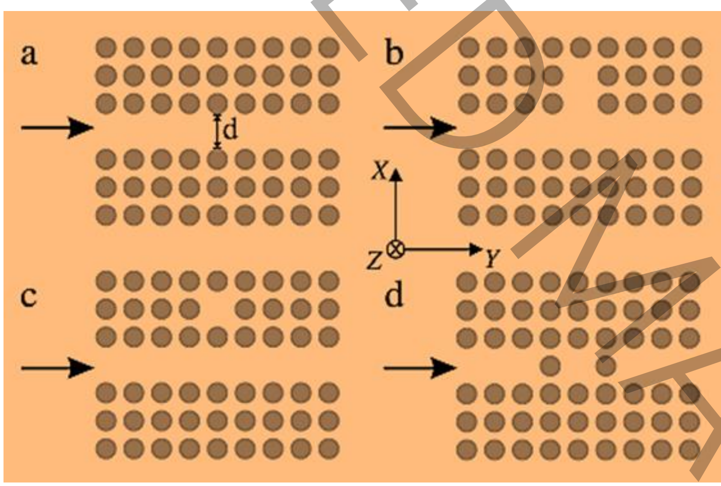


**Fig. 6 The 2D cross-sections of (a) a linear waveguide with the width of d, (b) A stub located vertically to the waveguide, (c) A side-coupled waveguide cavity, and (d) A cavity inside the linear waveguide, Ref. [123].**

The transmission and attenuation spectra due to the presence of cavities inside the waveguide path as well as outside the waveguide path are shown in Fig. 7. As can be seen from Fig. 7(a), the presence of cavities in the waveguide path causes a narrow passband in the transmission spectrum. On the other hand, the presence of these cavities outside the waveguide path and on one side of it, will cause a narrow attenuation band in the transmission spectrum at some frequencies. As a result, by changing the structure of the cavity, specific frequencies can be selected and passed or deleted.

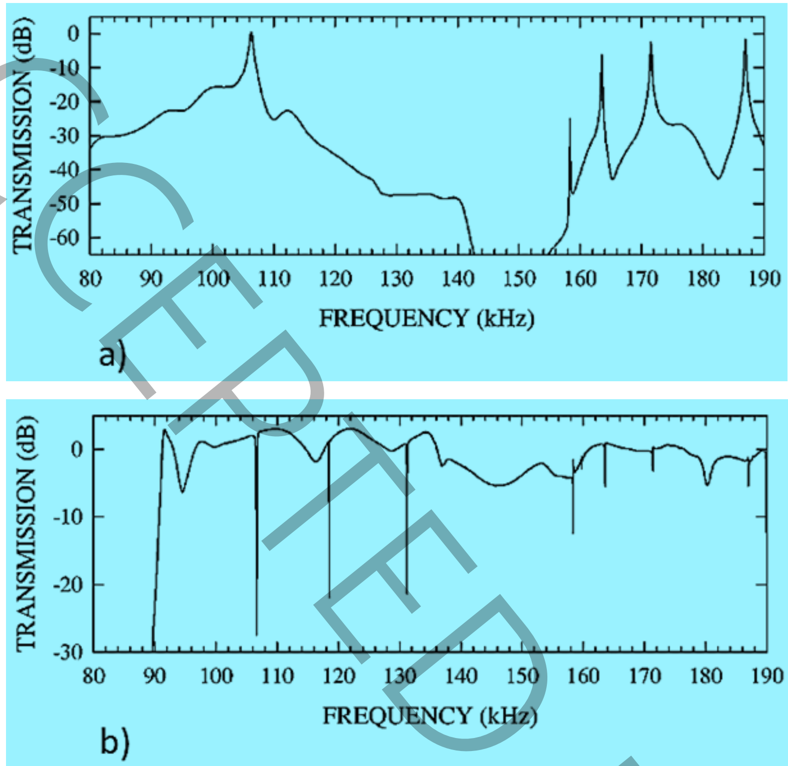


**Fig. 7. (a) Transmittance for Fig. 6(d) with *d*=11mm, (b) Transmittance for Fig. 6(c) with *d*=6.5mm, Ref. [123].**

In order to measure the transmission spectrum, the experimental setup is fabricated. The transmission spectrum of the perfect structure with a single point defect is measured in Fig. 8. According to Fig. 8(a), the defect mode occurs at a resonant frequency of $f_0$=287.7kHz. Then, two rods are removed in the propagation direction (*y* direction) and the transmission spectrum is examined in Fig. 8(b). It is observed that the localized mode for two-point defects is divided into two resonance modes with frequencies of $f_1$=280 and $f_2$=296.5kHz. The transmission spectrum for the two coupled cavities perpendicular to the *y* axis is shown in the Fig. 8(c). In this structure, the cavity modes are coupled and symmetrical, as in Fig. 8(b), except that the location of the *x* and *y* axes has changed. Although there are two separate modes, only one of them appears at a resonant frequency of $f_3$=279.3kHz. In fact, due to the longitudinal polarization in water, the mode which is anti-symmetrical relative to the *y* axis, cannot be excited[124].

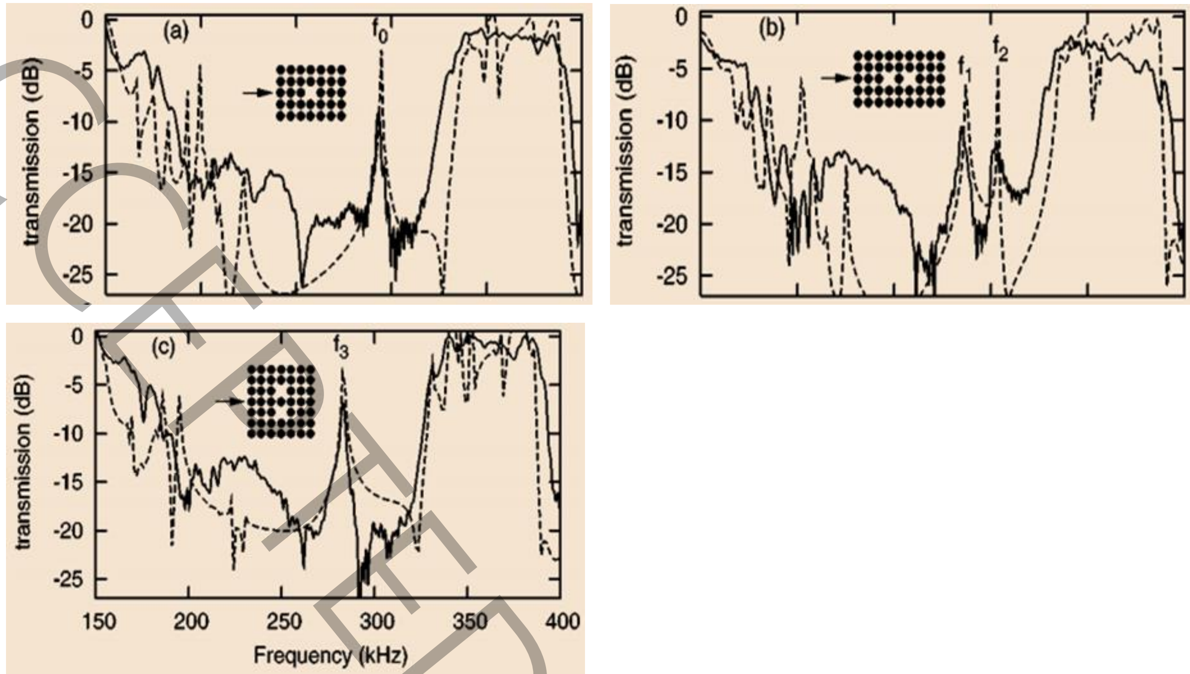


**Fig. 8. The transmission of Experimental (solid lines) and calculated (dashed lines). (a) a single defect induces a resonance mode with $f_0$. (b) Two defects in the propagation direction which make it has two split resonance modes at frequencies $f_1$ and $f_2$. (c) Two defects in perpendicular to the propagation direction, Ref[124].**

The line defects contain the hollow cylinders of smaller outer radius and high ratio for inner to outer radii make it possible to create narrow-band transmission spectra which can be suitable for designing the output waveguides of the demultiplexer. It should be noted that a defect containing a hollow cylinder of high outer radius can have a wide transmission. This property makes it possible to tune the frequency behavior by changing the inner to outer radii ratio[125,126].

It should be noted that the defects are divided to three kinds of geometry which are square defect, circular defect, and rectangular defect, respectively. for both square and circular defects, the modes of defects are only related to the defect filling fraction, however, in the rectangular defect, the defect modes could be tuned by changing the ratio of edge width of the defect[122]. For the bending waves, when a point defect is introduced, the bending waves are highly localized at or near the defect, leading to defect modes[127].

## 6 GUIDING

By removing one row of rods along the *x* axis (propagation direction), the straight waveguide ($W1$) is formed, which is shown in Fig. 9(a). The width $W1$ is the distance between neighboring rods on both sides of the waveguide. The transmission spectrum is shown in Fig. 10(a). According to this Fig., full transmission for acoustic waves at specific frequencies is seen within the stopband of PnC. It is observed that the confinement of the wave inside the waveguide is good enough and the propagation of the wave has low losses. It can be seen that the Finite Difference Time Domain (FDTD) calculations are in good agreement with the measurements[128].

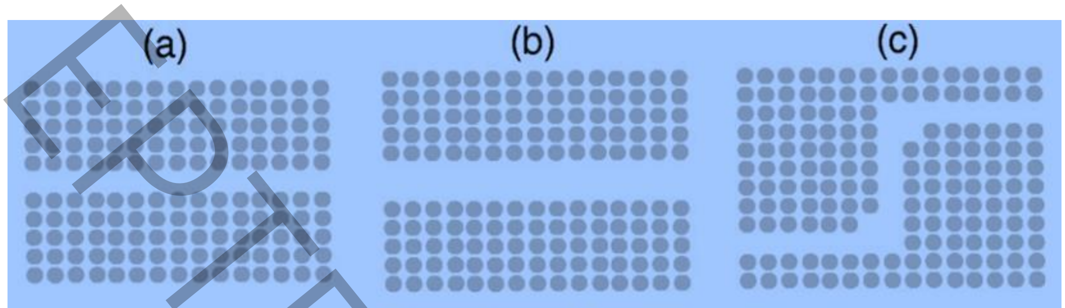


**Fig. 9. 2D cross-sections of (a) one-period wide straight waveguide (*W*1), (b) A two-period-wide straight waveguide (*W*2), and (c) A one-period-wide bent waveguide, Ref[128].**

The effect of changing the width of the waveguide has also been investigated and shown in Fig. 9(b). In this case, the two-row of rods are removed to form *W*2. The FDTD calculations, as well as the measured transmission, are shown in Fig. 10(b). It can be seen that two distinct waveguiding bands are located inside the stopband. There is also a strong attenuation at 285kHz. This is due to destructive interference at this frequency, which causes a stopband. The bending waveguide of 90° is also investigated in the *W*1 structure which is shown in Fig. 9(c). The two transmission drops to be seen around 281 and 299 kHz which is shown in Fig. 10(b). It can be concluded that the whole waveguiding band for bending waveguide covers about 70% of the full bandgap. The properties of the waveguides containing a row of hollow cylinders in a 2D PnC made of filled steel cylinders is investigated[129].

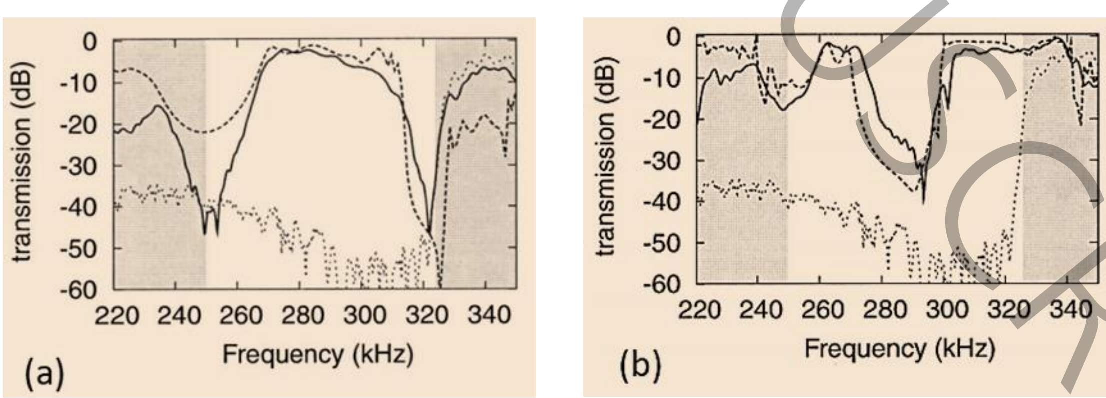

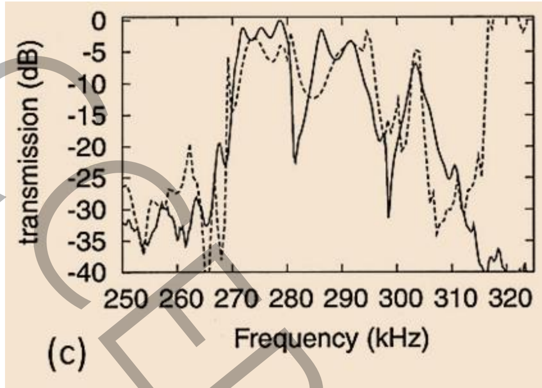


**Fig. 10. The transmission of Experimental (solid lines) and calculated (dashed lines). (a) the perfect crystal in the $\Gamma X$ direction for *W*1, (The gray areas delimit the full bandgap for the perfect crystal), (b) the perfect crystal in the $\Gamma X$ direction for *W*2, (c) the perfect crystal in the $\Gamma X$ direction for the one-period-wide bent waveguide, Ref[128].**

The wave propagation of acoustoelastic in 2D phononic epoxy metaplate is investigated. The coupled-resonator acoustoelastic waveguides (CRAEWs) formed in the perfect PnC metaplate by locally emptying certain cups[9]. Fig. 11(a) shows a straight line of defects with adjacent cavities which is separated by the two lattice constants. the phononic band structure of CRAEWs with the frequency response functions (FRF) are shown in Fig. 11(b-d) (numerical and experimental). It can be seen in the FRF that there are 10 dB differences between the experiments and the numerical simulations. This is due to the excitation sources of the simulations and experiments are not exactly the same. Fig. 11(e) shows the CRAEW supercell and the modal shape for the guided wave at point $N_L$.

The additional guiding bands in the frequency range of 8.09kHz to 8.27kHz are depicted in Fig. 11(b) which are very sensitive to local changes in the resonators. In this case, the coupling strength between the resonators defined the dispersion relationship. The out-of-plane displacement field for the finite sample for numerical (at 8.27kHz) and experiment (at 8.16 kHz) are shown in Fig. 11(f) and Fig. 11(g).

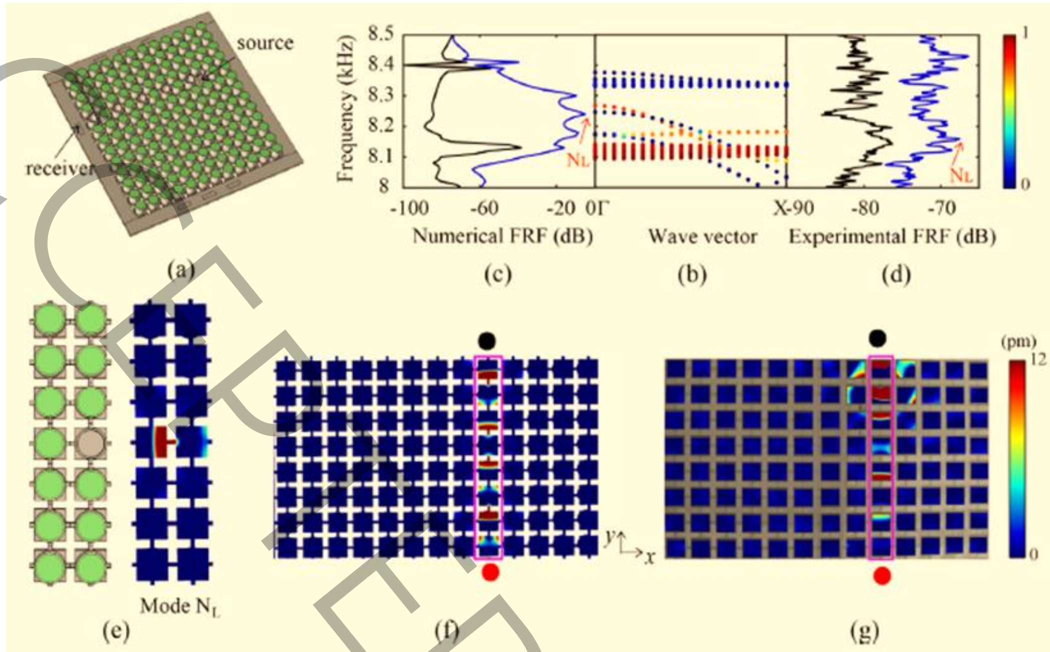


**Fig. 11. The wave propagation of acoustoelastic in 2D phononic epoxy metaplate is investigated.**
**(a) schematic of the epoxy metaplate with straight CRAEW formed by locally emptying a line of cups. The green is water and gray parts is epoxy materials. (b) band structure of perfect phononic metaplate with all cups filled with water (solid lines) and the straight CRAEW (dash lines) for a selected frequency range. (c) simulation and (d) experiment for the FRFs of the perfect phononic metaplate with all cups filled with water (black line) and for the straight CRAEW (blue line) (c) The CRAEW supercell and eigenmode $N_L$. (e) the numerical and (f) experimental and (g) out-of-plane displacement distributions are shown at 8.27 kHz and 8.16 kHz, respectively. The pink lines show the propagating circuits[9], Ref. [9].**

## 7 FILTERING

### 7.1 Acoustic Channel Drop Tunneling Using Point Defect Cavity

The acoustic channel drop tunneling in PnC based on point defect is shown in Fig. 12(a)[130]. The 2D square array of steel rods embedded in water to form the PnC structure. An appropriate coupling element is coupled between the two waveguides to transfer a specific wavelength. By removing the two rods (point defects) the stubs are formed as well as the two waveguides are composed of line defects.

The transmission of the structure is investigated on different ports which are shown in Fig. 12(b). By applying the input signal to port 1, a significant transmission peak is observed at port 3 at the frequency of 290 kHz. On the other hand, all the input signals in port 2 drops to zero and transfer to port 3, with a weak loss on port 4.

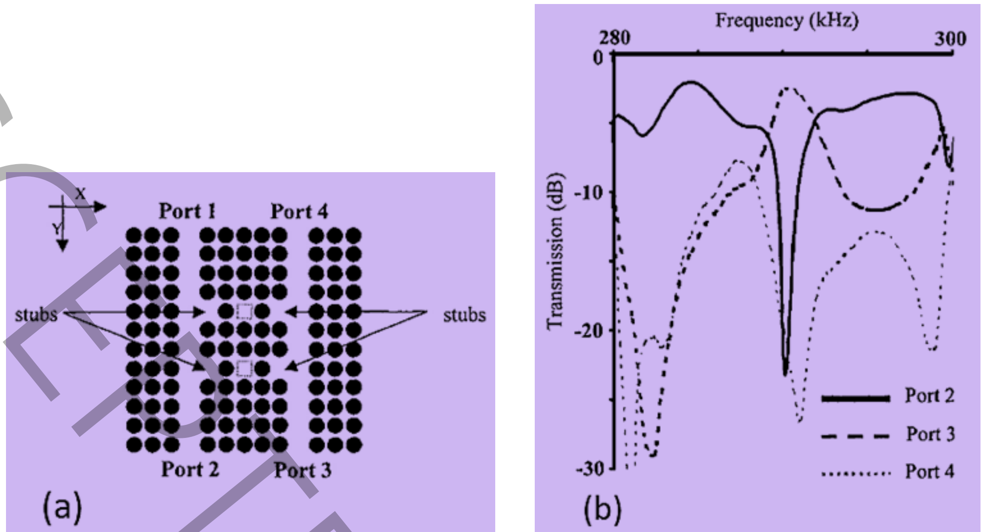


**Fig. 12. (a) Schematic of the Filter with the two stubs along the guides, and (b) Transmission for output ports of 2, 3, and 4, Ref.** [130]**.**

The effect of line defect and subs on the transmission spectrum are also investigated, separately. The waveguide has a wide passband in the range of 270<*f*<300kHz on which, the full transmission is observed in Fig. 13(a). By creating a point defect at the side of the waveguide, the stub is formed and causes to reject a narrow frequency in Fig. 13(b). It was also found that the single cavity inside the crystal cases to filtering of a narrow frequency band which is shown in Fig. 13(c). It should be noted that the resonances of both defects occur almost at the same frequency _f =290 kHz_, which again is in the favor of the coupling geometry shown in Fig. 12.

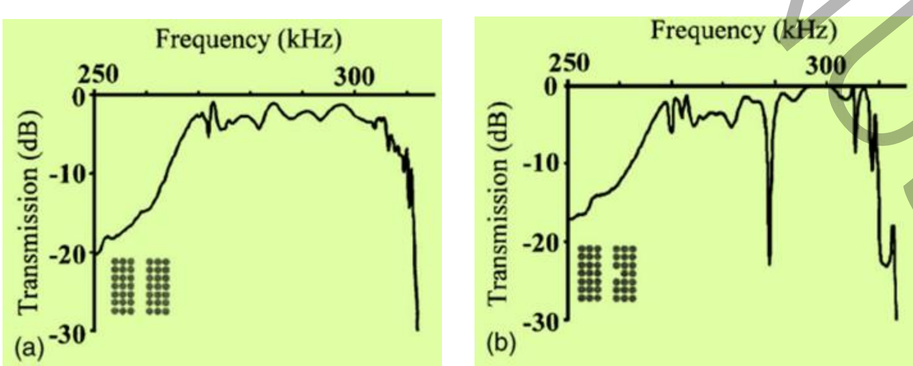

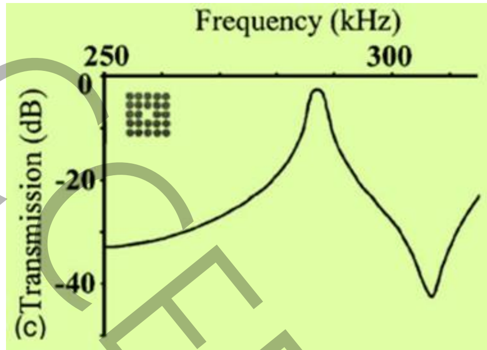


**Fig. 13. Transmission for (a) straight waveguide, (b) straight waveguide with the stub located at the side of the guide, and (c) single cavity inside the crystal, Ref. [130].**

### 7.2 Acoustic Add-drop Filter Using Ring Resonator

It is well known that ring resonators are very useful choices for filtering, reducing energy loss, and exhibiting high-quality factor[131]. The multimode nature of the ring resonator offers some advantages like flexibility in mode design and scalability in size[117,132]. It also has adaptability in structure design due to the multiple design parameters as compared to the point-defect resonator[130,133]. These reasons made the ring resonator to be used as a cavity and coupling element. Acoustic ring resonator containing surface modes of a 2D PnC was numerically investigated[134]. Employing spoof surface acoustic waves (SSAWs) as a compact RRs on the surface phononic crystals make them suitable for designing the 1D[135-137] and 2D[138,139] corrugations on solid slabs in which around the corrugations, energy is confined in air regions.

The general mechanism is that when the acoustic wave is circulating in a ring resonator, the wave amplitude is amplified due to the resonance phenomenon. Fig. 14(a) shows the structure of the add-drop filter using a ring resonator. In this structure, the water rods are embedded in the mercury matrix to form the PnC platform. Fig. 14(b) shows the transmission spectrum with the quality factor of $Q$≈1700. It can be seen that the four scatterer rods are added to the four corners of the structure. The presence of these four scatterer rods resulting in the so-called blue-shift in the frequency. This is due to it can suppress the nonresonant modes, and the wave rotation path inside the ring becomes smoother. It can also be observed that adding the mentioned rods causes to appear a dip in port C, which is centered around $f_0$=76.39kHZ. It means that the leakage in port C has been minimized[116].

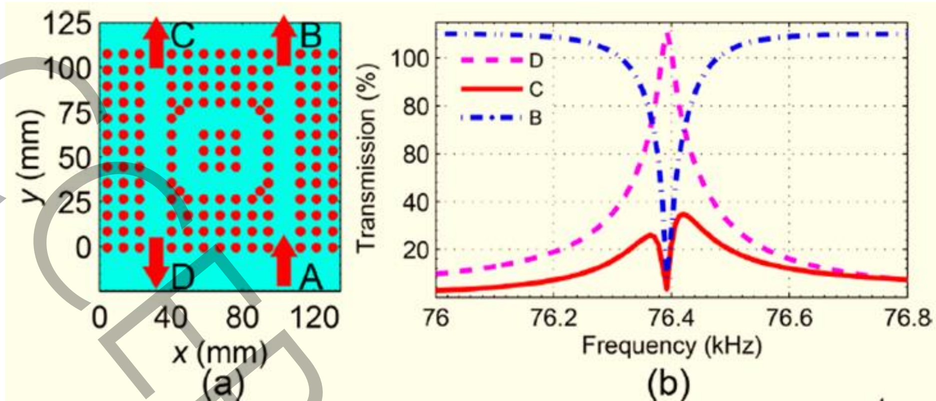


**Fig. 14. (a) Schematic and (b) the transmission of the add-drop filter, Ref. [116].**

In order to improve the performance in the design of the filter, some methods can be applied. The structure of the double-ring resonators channel drop filter (DRR-CDF) based on the phononic crystal is shown in Fig. 15(a). In this structure, the location of the left ring resonator is shifted upwards as much as a row of rods. Fig. 15(b) shows the transmission spectrum with the quality factor of $Q\approx2000$. It can be observed that the capability of ultrafine tuning of the output resonant frequency, as well as fine-tuning the output port, was done by changing the location of each ring. All details about the mentioned method are given in Ref[140].

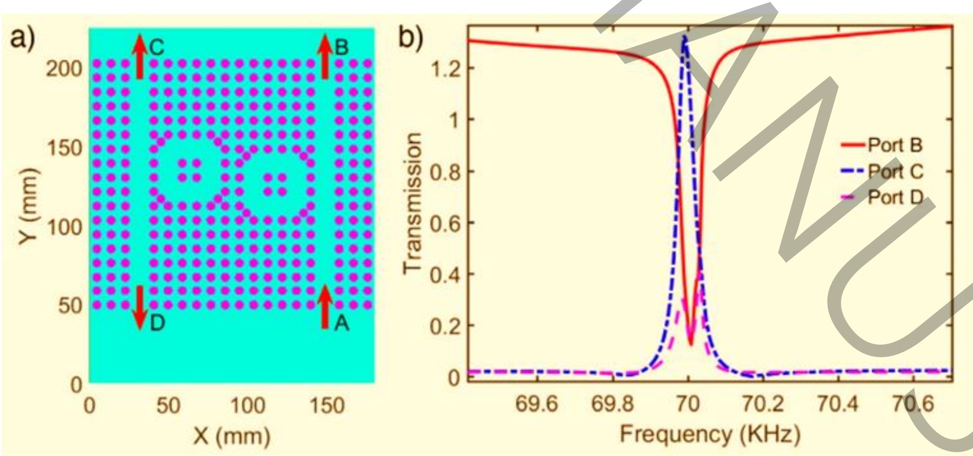


**Fig. 15. Schematic (a) and the transmission (b) of double-ring resonators channel drop filter (DRR-CDF), Ref. [140].**

## 8 DEMULTIPLEXING

### 8.1 Tunable Four-channel Acoustic Demultiplexer Using Point Defect Cavity

It is well known that the addition of point defects to the perfect PnCs gives them unique abilities for the design of many PnC based acoustic devices like waveguides and cavities to enable novel functionalities in a compact structure. In the point defect cavity, the eigenmodes can be used to induce either narrow passing bands in the stopband or narrow stopping bands within the passband[116,129,132]. The structure of the demultiplexer with point defect cavity and its transmission spectrum is shown in Fig. 16(a) and (b). This structure contains four cylindrical cavities filled with methyl nonafluorobutyl ether (MNE) that each cylinder has a different radius. The difference in dimension of the four arms makes it possible to have demultiplexing functionality[141]. The demultiplexer structure includes four different cavities are also investigated[142].

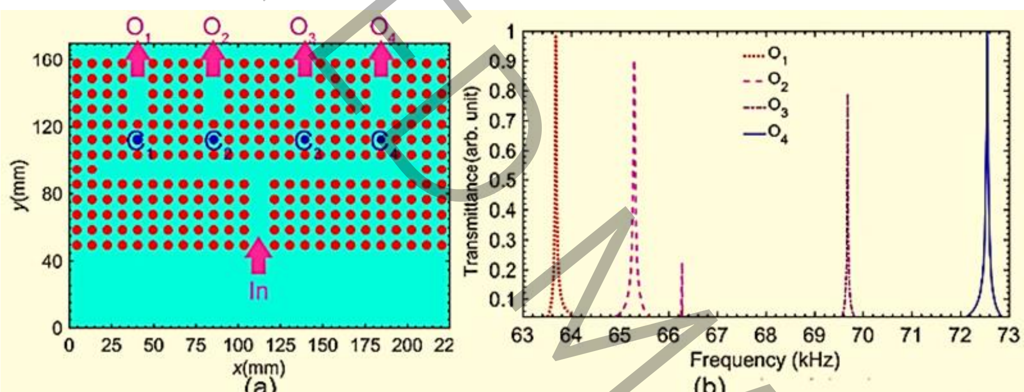


**Fig. 16. Schematic (a) and the transmission (b) of four-channel acoustic demultiplexer, Ref. [141].**

### 8.2 Acoustic Switchable Demultiplexer

Fig. 17(a) shows the structure in which the two arms are coupled to two output ports by two dissimilar point defect cavities ($C_L$, $C_R$) and two different resonant frequencies ($f_L$, $f_R$), filled with methyl nonafluorobutyl ether (MNE) and ethyl nonafluorobutyl ether (ENE). The difference in acoustic properties of these two materials causes the cavities resonant modes to be different, required for the demultiplexing functionality. It should be pointed out that choosing two different temperatures for the two cavities makes the structure can act as an acoustic switch too. Fig. 17(b) shows the effect of the temperature dependence of point defects on the resonant frequencies of cavity, in which the transmission peaks are switched. When the temperature changes, the speed of sound and mass density will change. As a result, the output frequency will change. Switch-ability is expressed as the temperatures at which the center frequency of MNE ($C_L$) switches with that of ENE ($C_R$), and vice versa. It means that by setting the specific temperature for MNE and ENE ($C_L$=19°C, $C_R$=31.6°C), the frequencies of output channels can switch to the new conditions[132]. The switchable demultiplexer which have improved dual separating and switching performances are investigated[142].

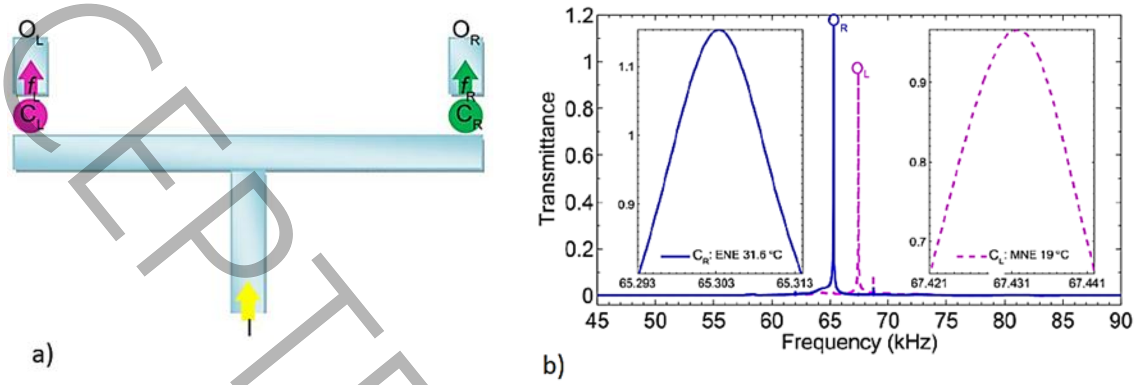


**Fig. 17. Schematic (a) and (b) the transmission of the acoustic demultiplexer. The temperature for MNE and ENE are set at 19°C and 31.6°C, respectively. $C_L$ and $C_R$ are the point defect cavities and $f_L$ and $f_R$ are resonant frequencies for left and right, respectively, Ref. [132].**

### 8.3 Acoustic 1×2 Demultiplexer Using Ring Resonator

Taking advantage of the basic idea in using the ring resonator which is mentioned earlier, an acoustic demultiplexer is designed. The scheme and the transmission spectrum of 1×2 demultiplexer, having two output channels, are shown in Fig. 18(a) and (b). In this structure, the acoustic wave rotates inside the ring resonator and the amplitude of the wave can be amplified by the resonance phenomenon. By changing the physical and geometrical properties of inclusions, the effective path length of the acoustic wave is varied. The quality factors ($Q$) of the structure are $Q_1$=3997 and $Q_2$=8145 which are centered around 63.960kHz and 73.312kHz[117]. The heterostructure demultiplexer based on solid-solid PnC ring resonators in the range of GHz is investigated. In this structure, they achieved very high average quality factor of 4570 among the output channels[118].

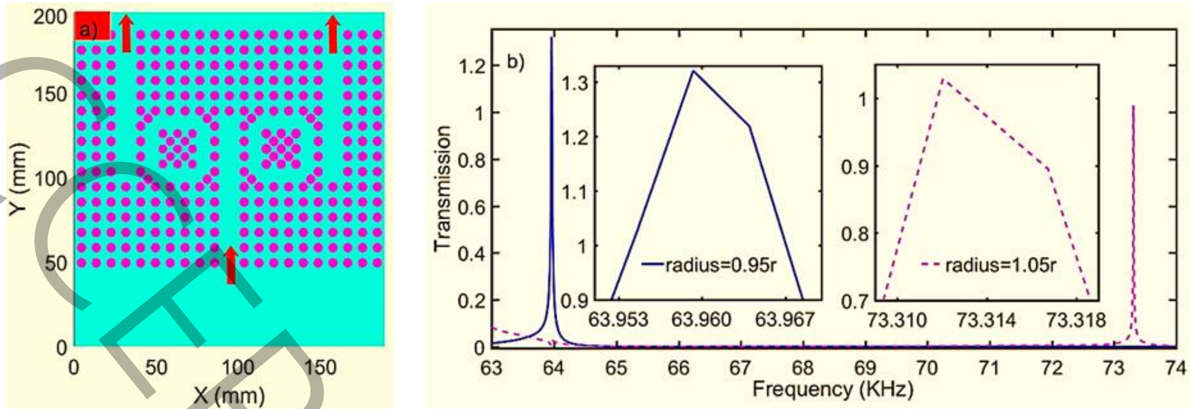


**Fig. 18. Schematic (a) and (b) the transmission of acoustic demultiplexer using two different ring resonators. The left radius is 0.95*r* and the right radius is 1.05*r*, Ref. [117].**

9 CONCLUSIONS

To conclude, PnCs are one of the most critical platforms of the future acoustic integrated circuits containing waveguides and cavities. Recent devices are more promising for controlling and manipulating acoustic waves. In this regard, different types of PnCs, e.g., solid-solid, solid-liquid, and liquid-liquid in comparison to the PC was investigated. It is proved that by changing the structure of the cavity through point defects and line defect, specific frequencies can be selected and passed or rejected. The effect of changing the width of the waveguide causes two distinct waveguiding bands which are located inside the stopband. The multimode nature of the ring resonator makes it has scalability in size, adaptability in structure design and flexibility in mode design in comparison to the point-defect resonator which are the reasons for using them as a cavity and coupling element. In these studies, the lattice constant of the structures is a = 9mm and the filling fraction of ff = 0.3 and the interested range of frequency falls within 43 KHz to 119 kHz which is suitable for practical guiding applications. The Interchannel crosstalks for the demultiplexer is less than−32 dB and also the quality factors for each port of this system are Q1 = 3997 and Q2 = 8145. On the other hand, the quality factor for the filter is Q = 2000. The main object of this study was to present the basic results about fabrication process, defects and band gaps in phononic crystals, as well as the related equations in FDTD method. Besides the guiding, filtering, demultiplexing properties and their functionalities in acoustic devices have been widely studied. With such a platform, it is possible to have tunable acoustic devices based on PnCs.

**Conflicts of Interest**

The authors declare that they have no conflict of interest.

**Author Contribution**

Amir Rostami (AR)
Babak Rostami-dogolsara (BR)
Hassan Kaatuzian (HK)

AR and BR conceived of the presented idea. They are also were involved in planning the work. AR wrote the manuscript with support from HK and BR. HK encouraged team to investigate and supervised the findings of this work. All authors discussed the results and contributed to the final manuscript.

**Abbreviation List**

| | |
|---|---|
| CRAEW | Coupled-Resonator Acoustoelastic Waveguides |
| DRR-CDF | Double-Ring Resonators Channel Drop Filter |
| ENE | Ethyl Nonafluorobutyl Ether |
| FRF | Frequency Response Functions |
| FDTD | Finite Difference Time Domain |
| GRIN PC | Gradient-index Phononic Crystal |
| MNE | Methyl Nonafluorobutyl Ether |
| MEMS | Micro-Electromechanical System |
| NEMS | Nano-Electromechanical System |
| PnC/PC | Phononic crystal |
| PtC | Photonic crystal |
| PnBG | Phononic Band Gag |
| SOI | Silicon on Insulator |
| SSAW | Spoof Surface Acoustic Wave |
| ZnO | Zinc oxide |

**References**

[1] Yablonovitch E. Inhibited Spontaneous Emission in Solid-State Physics and Electronics. Physical Review Letters, 58 (1987) 2059.

[2] Sigalas MM, Economou EN. Elastic and acoustic wave band structure. Journal of Sound and Vibration, 158 (1992) 377-382.

[3] Kushwaha MS, Halevi P, Dobrzynski L et al. Acoustic band structure of periodic elastic composites. Physical Review Letters, 71 (1993) 2022.

[4] Sigalas M, Economou EN. Band structure of elastic waves in two dimensional systems. Solid State Communications, 86 (1993) 141-143.

[5] Davis BL, Hussein MI. Nanophononic Metamaterial: Thermal Conductivity Reduction by Local Resonance. Physical Review Letters, 112 (2014) 055505.

[6] Wang YF, Wang TT, Wang YS et al. Reconfigurable Phononic-Crystal Circuits Formed by Coupled Acoustoelastic Resonators. Physical Review Applied, 8 (2017) 014006.

[7] Zhang X, Qu Z, Tian D et al. Acoustic characteristics of continuously graded phononic crystals. Applied Acoustics, 151 (2019) 22-29.

[8] Van den Boom SJ, Abedi R, van Keulen F et al. A level set-based interface-enriched topology optimization for the design of phononic crystals with smooth boundaries. Computer Methods in Applied Mechanics and Engineering, 408 (2023) 115888.

[9] Wang TT, Wang YF, Deng ZC et al. Reconfigurable coupled-resonator acoustoelastic waveguides in fluid-filled phononic metaplates. Composite Structures, 303 (2023) 116355.

[10] Laude V, Achaoui Y, Benchabane S et al. Evanescent Bloch waves and the complex band structure of phononic crystals. Physical Review B, 80 (2009) 092301.

[11] Miranda Jr E, Dos Santos J. Evanescent Bloch waves and complex band structure in magneto-electroelastic phononic crystals. Mechanical Systems and Signal Processing, 112 (2018) 280-304.

[12] Wang YF, Zhang SY, Wang YS et al. Hybridization of resonant modes and Bloch waves in acoustoelastic phononic crystals. Physical Review B, 102 (2020) 144303.

[13] Gao N, Wang B, Lu K et al. Complex band structure and evanescent Bloch wave propagation of periodic nested acoustic black hole phononic structure. Applied Acoustics, 177 (2021) 107906.

[14] Miranda Jr E, Rodrigues S, Dos Santos J. Complex dispersion diagram and evanescent modes in piezomagnetic phononic structures. Solid State Communications, 346 (2022) 114697.

[15] Jiang T, Han Q, Li C. Complex band structure and evanescent wave propagation of composite

corrugated phononic crystal beams. Acta Mechanica, 234 (2023) 2783-2808.
[16] Laude V. Phononic Crystals: Artificial Crystals for Sonic, Acoustic, and Elastic Waves. Berlin, Boston: De Gruyter, (2020).
[17] Jin Y, Djafari-Rouhani B, Torrent D. Gradient index phononic crystals and metamaterials. Nanophotonics, 8 (2019) 685-701.
[18] Vasileiadis T, Varghese J, Babacic V et al. Progress and perspectives on phononic crystals. Journal of Applied Physics, 129 (2021) 160901.
[19] Benchabane S, Khelif A, Daniau W et al. Silicon phononic crystal for surface acoustic waves. 2005 IEEE Ultrasonics Symposium, n/a(n/a) (2005) 922-925.
[20] Wang YZ, Wang YS. Active control of elastic wave propagation in nonlinear phononic crystals consisting of diatomic lattice chain. Wave Motion, 78 (2018) 1-8.
[21] Arretche I, Matlack KH. Effective phononic crystals for non-Cartesian elastic wave propagation. Physical Review B, 102 (2020) 134308.
[22] Chen Z, Wang G, Zhou W et al. Elastic foundation induced wide bandgaps for actively-tuned topologically protected wave propagation in phononic crystal beams. International Journal of Mechanical Sciences, 194 (2021) 106215.
[23] Gao N, Qu S, Si L et al. Broadband topological valley transport of elastic wave in reconfigurable phononic crystal plate. Applied Physics Letters, 118 (2021) 063502.
[24] Shao H, Chen G, He H. Elastic wave localization and energy harvesting defined by piezoelectric patches on phononic crystal waveguide. Physics Letters A, 403 (2021) 127366.
[25] Song Y, Shen Y. A tunable phononic crystal system for elastic ultrasonic wave control. Applied Physics Letters, 118 (2021) 224104.
[26] Zhou X, Sun Y, Yang S et al. Band gap manipulation on P-wave propagating in functionally graded phononic crystal by periodical thermal field. International Journal of Mechanical Sciences, 212 (2021) 106817.
[27] Huo SY, Xie GH, Qiu SJ et al. Broadband valley-locked waveguide states of elastic wave in topological phononic crystal plates with asymmetric double-sided pillars. Mechanics of Advanced Materials and Structures, 29 (2022) 7772-7780.
[28] Yao LC, Hsieh KH, Chiu SC et al. Frequency-selective valley edge routing of elastic wave in topological phononic crystals with different symmetries. Journal of Physics: Condensed Matter, 35 (2023) 205701.
[29] Wang YF, Wang YZ, Wu B et al. Tunable and active phononic crystals and metamaterials. Applied Mechanics Reviews, 72 (2020) 040801.
[30] Kushwaha MS, Halevi P, Martinez G et al. Theory of acoustic band structure of periodic elastic

composites. Physical Review B, 49 (1994) 2313.
[31] Qi XQ, Li TJ, Zhang JL et al. Band gap structures for 2D phononic crystals with composite scatterer. Applied Physics A, 124 (2018) 1-7.
[32] Fomenko SI, Golub MV, Chen A et al. Band-gap and pass-band classification for oblique waves propagating in a three-dimensional layered functionally graded piezoelectric phononic crystal. Journal of Sound and Vibration, 439 (2019) 219-240.
[33] Yang G, Zhang M, Hu J et al. Effects of initial stress on band gap of Love waves in a layered domain-inverted phononic crystal structure. Ultrasonics, 106 (2020) 106145.
[34] Alam Z, Sharma AK. Functionally Graded Soft Dielectric Elastomer Phononic Crystals: Finite Deformation, Electro-Elastic Longitudinal Waves, and Band Gaps Tunability via Electro-Mechanical Loading. International Journal of Applied Mechanics, 14 (2022) 2250050.

[35] Guo J, Zhang Z. Mass inertia moment-based design of band gap characteristics in zigzag beam-supported stepped phononic crystals. Applied Physics A, 128 (2022) 126.
[36] Jin J, Hu N, Hu H. Investigation of size effect on band structure of 2D nano-scale phononic crystal based on nonlocal strain gradient theory. International Journal of Mechanical Sciences, 219 (2022) 107100.
[37] Li Y, Luo Y, Zhang X. Topological design of phononic crystals for multiple wide band gaps. Journal of Sound and Vibration, 529 (2022) 116962.
[38] Mehaney A, Ahmed AM, Elsayed HA et al. Hydrostatic pressure effects for controlling the phononic band gap properties in a perfect phononic crystal. Optical and Quantum Electronics, 54 (2022) 94.
[39] Qian D, Zou P, Zhang J et al. Tunability of resonator with pre-compressed springs on thermo-magneto-mechanical coupling band gaps of locally resonant phononic crystal nanobeam with surface effects. Mechanical Systems and Signal Processing, 176 (2022) 109184.
[40] Wang Y, Guo J, Zhang Z. The deformation induced tunable topology in controlling of band gap characteristics for stepped phononic crystals. Solid State Communications, 35 (2022) 114809.
[41] Willey CL, Chen VW, Roca D et al. Coiled Phononic Crystal with Periodic Rotational Locking: Subwavelength Bragg Band Gaps. Physical Review Applied, 18 (2022) 014035.
[42] Jin Y, Torrent D, Djafari-Rouhani B. Robustness of conventional and topologically protected edge states in phononic crystal plates. Physical Review B, 98 (2018) 054307.
[43] Li X, Meng Y, Wu X et al. Su-Schrieffer-Heeger model inspired acoustic interface states and edge states. Applied Physics Letters, 113 (2018) 203501.
[44] Liu TW, Semperlotti F. Tunable acoustic valley-hall edge states in reconfigurable phononic elastic waveguides. Physical Review Applied, 9 (2018) 014001.
[45] Mei J, Wang J, Zhang X et al. Robust and high-capacity phononic communications through topological

edge states by discrete degree-of-freedom multiplexing. Physical Review Applied, 12 (2019) 054041.
[46] Wang W, Bonello B, Djafari-Rouhani B et al. Topological valley, pseudospin, and pseudospin-valley protected edge states in symmetric pillared phononic crystals. Physical Review B, 100 (2019) 140101.
[47] Sui F, Chen J, Huang H. Tunable topological edge states and rainbow trapping in two dimensional magnetoelastic phononic crystal plates based on an external magnetostatic field. International Journal of Mechanical Sciences, 225 (2022) 107360.
[48] Tian Y, Zhang W, Tan Z et al. Chiral edge states for phononic crystals based on shunted piezoelectric materials. Extreme Mechanics Letters, 50 (2022) 101568.
[49] Xia B, Zhang J, Tong L et al. Topologically valley-polarized edge states in elastic phononic plates yielded by lattice defects. International Journal of Solids and Structures, 239, (2022) 111413.
[50] Schriemer HP, Cowan ML, Page JH et al. Energy velocity of diffusing waves in strongly scattering media. Physical Review Letter, 79 (1997) 3166.
[51] Zhu X, Li K, Zhang P et al. Implementation of dispersion-free slow acoustic wave propagation and phase engineering with helical-structured metamaterials. Nature Communications, 7 (2016) 11731.
[52] Korozlu N, Kaya O, Cicek A et al. Self-collimation and slow-sound effect of spoof surface acoustic waves. Journal of Applied Physics, 125 (2019) 074901.
[53] Achilleos V, Auregan Y, Pagneux V. Using slow sound to achieve unidirectional acoustic propagation. 28th AIAA/CEAS Aeroacoustics 2022 Conference, n/a(n/a) (2022) 2899.
[54] Martin R, Schuermans B, Noiray N. Experimental investigation of a phase-cancelling slow-sound metamaterial with mean flow. INTER-NOISE and NOISE-CON Congress and Conference Proceedings, 2022.
[55] Chua JW, Li X, Yu X et al. Novel slow-sound lattice absorbers based on the sonic black hole. Composite Structures, 304 (2023) 116434.
[56] El kadmiri I, Ben-Ali Y, Khaled A et al. Acoustic filtering and guiding by the presence of a defect at the opened resonators level's in one-dimensional comb-like phononic structure. Materials Today: Proceedings 31 (2020) S33-S40.
[57] El Kadmiri I, Ben-Ali Y, Ouariach A et al. Double Frequency Filtering in One Dimensional Comb-Like Phononic Structure Containing a Segment Defect. In: Saka A et al. Advances in Integrated Design and Production. CPI 2019. Lecture Notes in Mechanical Engineering. Springer, Cham, 2021.
[58] Jo SH, Yoon H, Shin YC et al. Revealing defect-mode-enabled energy localization mechanisms of a one-dimensional phononic crystal. International Journal of Mechanical Sciences, 215 (2022) 106950.
[59] Kingsley AD, Anderson BE, Ulrich TJ. Super-resolution within a one-dimensional phononic crystal of resonators using time reversal in an equivalent circuit model. Journal of the Acoustical Society of America, 152 (2022) 1263-1271.

[60] Lu L, Ma D, Zhong M et al. Temperature oscillation in one-dimensional superlattice induced by phonon localization. New Journal of Physics, 24 (2022) 013007.
[61] Mkaoir M, Ketata H, Njeh A. Lamb waves propagating in one-dimensional phononic composite and nesting Fibonacci piezoelectric superlattices plate coated on a uniform substrate. Mechanics of Advanced Materials and Structures, 29 (2022) 3623-3632.
[62] Zhang H, Zhang S, Liu J et al. Synthetic weyl points of the shear horizontal guided waves in one-dimensional phononic crystal plates. Applied Sciences, 12 (2022) 167.
[63] Wu X, Ying P, Li C et al. Dual effects of hetero-interfaces on phonon thermal transport across graphene/C3N lateral superlattices. International Journal of Heat and Mass Transfer, 201 (2023) 123643.
[64] Ghoreshi M, Bahrami A. Acoustic invisibility cloak based on two-dimensional solid-fluid phononic crystals. Solid State Communications, 342 (2022) 114646.
[65] Marunin MV, Polikarpova NV. Polarization of Acoustic Waves in Two-Dimensional Phononic Crystals Based on Fused Silica. Materials, 15 (2022) 8315.
[66] Mukhin N, Kutia M, Aman A et al. Two-dimensional phononic crystal based sensor for characterization of mixtures and heterogeneous liquids. Sensors, 22 (2022) 2816.
[67] Sun XW, Zhu HF, Gao XL et al. Tunable low-frequency bandgaps of a new two-dimensional multi-component phononic crystal under different pressures, geometric parameters and pre-compression strains. Mechanics of Advanced Materials and Structures, 29 (2022) 4019-4031.
[68] Wang TT, Wang YF, Deng ZC et al. Reconfigurable waveguides defined by selective fluid filling in two-dimensional phononic metaplates. Mechanical Systems and Signal Processing, 165 2022) 108392.
[69] Li W, Sun L, Gu Y et al. Singular boundary method for band structure calculations of in-plane waves in 2D phononic crystals. Engineering Analysis with Boundary Elements, 146 (2023) 204-215.
[70] Flores Méndez J, Pinón Reyes AC, Heredia Jiménez AH et al. Discretization Approach for the Homogenization of Three-Dimensional Solid-Solid Phononic Crystals in the Quasi-Static Limit: Density and Elastic Moduli. Applied Sciences, 12 (2022) 2987.
[71] Gantasala S, Thomas T, Rajagopal P. Spherical Inclusions Based Defect Modes in a Phononic Crystal for Piezoelectric Energy Harvesting. In: Rizzo P, Milazzo A (eds). European Workshop on Structural Health Monitoring. EWSHM 2022. Lecture Notes in Civil Engineering, Springer, Cham. n/a(n/a) (2022) 952-962.
[72] Liu JJ, Li ZW, Chen ZG et al. Experimental Realization of Weyl Exceptional Rings in a Synthetic Three-Dimensional Non-Hermitian Phononic Crystal. Physical Review Letters, 129 (2022) 084301.
[73] Aravantinos-Zafiris N, Sigalas MM, Katerelos DT. Complete acoustic bandgaps in a three-dimensional phononic metamaterial with simple cubic arrangement. Journal of Applied Physics, 133 (2023) 065101.
[74] Gao H, Qu Y, Meng G. Topology Optimization and Wave Propagation of Three-Dimensional Phononic Crystals. Journal of Vibration and Acoustics, 145 (2023) 011002.

[75] Yip KL, John S. Resonance gaps and slow sound in three-dimensional phononic crystals: Rod-in-a-box paradigm. Physical Review B, 107 (2023) L060306.

[76] Landau LD. EM Lifshitz Theory of elasticity. Course of Theoretical Physics, 7 (1986).

[77] Olsson RH, El-Kady I. Microfabricated phononic crystal devices and applications. Measurement Science and Technology, 20 (2008) 012002.

[78] Khelif A, Adibi A. Phononic Crystals. Berlin, Germany, Springer, (2015).

[79] Maldovan M. Sound and heat revolutions in phononics. Nature, 503 (2013) 209-217.

[80] Miyashita T, Sato W, Nakaso Y et al. Experimental studies on two-dimensional defect-mode waveguides in a sonic/phononic crystal. Japanese Journal of Applied Physics, 46 (2007) 4684.

[81] Hladky-Hennion AC, Vasseur J, Djafari-Rouhani B et al. Sonic band gaps in one-dimensional phononic crystals with a symmetric stub. Physical Review B, 77 (2008) 1104304.

[82] Oudich M, Li Y, Assouar BM et al. A sonic band gap based on the locally resonant phononic plates with stubs. New Journal of Physics, 12 (2010) 083049.

[83] Walker E, Reyes D, Rojas MM et al. Tunable ultrasonic phononic crystal controlled by infrared radiation. Applied Physics Letters, 105 (2014) 143503.

[84] Li Z, Yang S, Wang D et al. Focus of ultrasonic underwater sound with 3D printed phononic crystal. Applied Physics Letters, 119 (2021) 073501.

[85] Jo SH, Youn BD. Enhanced ultrasonic wave generation using energy-localized behaviors of phononic crystals. International Journal of Mechanical Sciences, 228 (2022) 107483.

[86] Alonso-Redondo E, Schmitt M, Urbach Z et al. A new class of tunable hypersonic phononic crystals based on polymer-tethered colloids. Nature Communications, 6 (2015) 8309.

[87] Sledzinska M, Graczykowski B, Maire J et al. 2D phononic crystals: Progress and prospects in hypersound and thermal transport engineering. Advanced Functional Materials, 30 (2020) 1904434.

[88] Florez O, Arregui G, Albrechtsen M et al. Engineering nanoscale hypersonic phonon transport. Nature Nanotechnology, 17 (2022) 947-951.

[89] Hopkins PE, Phinney LM, Rakich PT et al. Phonon considerations in the reduction of thermal conductivity in phononic crystals. Applied Physics A, 103 (2011) 575-579.

[90] Yang L, Yang N, Li B. Extreme Low Thermal Conductivity in Nanoscale 3D Si Phononic Crystal with Spherical Pores. Nano Letters, 14 (2014) 1734-1738.

[91] Masrura HM, Kareekunnan A, Liu F et al. Design of Graphene Phononic Crystals for Heat Phonon Engineering. Micromachines, 11 (2020) 655.

[92] Croënne C, Manga ED, Morvan B et al. Negative refraction of longitudinal waves in a two-dimensional solid-solid phononic crystal. Physical Review B, 83 (2011) 054301.

[93] Reinke CM, Su MF, Olsson RH et al. Realization of optimal bandgaps in solid-solid, solid-air, and

hybrid solid-air-solid phononic crystal slabs. Applied Physics Letter, 98 (2011) 061912.
[94] Morvan B, Tinel A, Vasseur JO et al. Ultra-directional source of longitudinal acoustic waves based on a two-dimensional solid/solid phononic crystal. Journal of Applied Physics, 16 (2014) 214901.
[95] Liu ZF, Wu B, He CF. Systematic topology optimization of solid-solid phononic crystals for multiple separate band-gaps with different polarizations. Ultrasonics, 65 (2016) 249-257.
[96] Wei Q, Xiang J, Zhu W et al. WBEM-based analysis of band structures of solid-solid and fluid-fluid phononic crystals with frequency-independent fundamental solutions. Engineering Analysis with Boundary Elements, 151 (2023) 439-456.
[97] Albuquerque EL, Sesion PD. Band gaps of acoustic waves propagating in a solid/liquid phononic Fibonacci structure. Physica B, 405 (2010) 3704-3708.
[98] Oseev A, Mukhin N, Lucklum R et al. Study of liquid resonances in solid-liquid composite periodic structures (phononic crystals)-theoretical investigations and practical application for in-line analysis of conventional petroleum products. Sensors and Actuators B: Chemical, 257 2018 469-477.
[99] Mukhin N, Kutia M, Oseev A et al. Narrow band solid-liquid composite arrangements: Alternative solutions for phononic crystal-based liquid sensors. Sensors, 19 (2019) 3743.
[100] Walton F, Bolling J, Farrell A et al. Polyamorphism Mirrors Polymorphism in the Liquid–Liquid Transition of a Molecular Liquid. Journal of the American Chemical Society, 142 (2020) 7591-7597.
[101] Park JH, Ma PS, Kim YY. Design of phononic crystals for self-collimation of elastic waves using topology optimization method. Structural and Multidisciplinary Optimization, 51 (2015) 1199-1209.
[102] Jia Z, Luo Y, Takezawa A et al. Topology optimization for realizing tailored self-collimation in phononic crystals. International Journal for Numerical Methods in Engineering, 123 (2022) 4170-4182.
[103] He J, Kang Z. Achieving directional propagation of elastic waves via topology optimization. Ultrasonics, 82 (2018) 1-10.
[104] Xie L, Xia B, Huang G et al. Topology optimization of phononic crystals with uncertainties. Structural and Multidisciplinary Optimization, 56 (2017) 1319-1339.
[105] Zhang X, He J, Takezawa A et al. Robust topology optimization of phononic crystals with random field uncertainty. International Journal for Numerical Methods in Engineering, 115 (2018) 1154-1173.
[106] Zhang X, Takezawa A, Kang Z. A phase-field based robust topology optimization method for phononic crystals design considering uncertain diffuse regions. Computational Materials Science, 160 (2019) 159-172.
[107] Yi G, Youn BD. A comprehensive survey on topology optimization of phononic crystals. Structural and Multidisciplinary Optimization, 54 (2016) 1315-1344.
[108] Vatanabe SL, Paulino GH, Silva EC. Maximizing phononic band gaps in piezocomposite materials by means of topology optimization. Journal of the Acoustical Society of America, 136 (2014) 494-501.

[109] Chen Y, Guo D, Li YF et al. Maximizing wave attenuation in viscoelastic phononic crystals by topology optimization. Ultrasonics, 94 (2019) 419-429.

[110] Hedayatrasa S, Abhary K, Uddin M et al. Optimum design of phononic crystal perforated plate structures for widest bandgap of fundamental guided wave modes and maximized in-plane stiffness. Journal of the Mechanics and Physics of Solids, 89 (2016) 31-58.

[111] Liu J, Guo H, Wang T. A review of acoustic metamaterials and phononic crystals. Crystals, 10 (2020) 305.

[112] Zhang S. Acoustic metamaterial design and applications. University of Illinois at Urbana-Champaign, Ph.D. Dissertation, (2010).

[113] Sigalas M, Kushwaha MS, Economou EN et al. Classical vibrational modes in phononic lattices: theory and experiment. Zeitschrift für Kristallographie-Crystalline Materials, 220 (2005) 765-809.

[114] Mohammadi S, Eftekhar AA, Khelif A et al. Evidence of large high frequency complete phononic band gaps in silicon phononic crystal plates. Applied Physics Letter, 92 (2008) 221905.

[115] Chiou MJ, Lin YC, Ono T et al. Focusing and waveguiding of Lamb waves in micro-fabricated piezoelectric phononic plates. Ultrasonics, 54 (2014) 1984-1990.

[116] Rostami-Dogolsara B, Moravvej-Farshi MK, Nazari F. Acoustic add-drop filters based on phononic crystal ring resonators. Physical Review B, 93 (2016) 014304.

[117] Rostami A, Kaatuzian H, Rostami-Dogolsara B. Acoustic 1×2 demultiplexer based on fluid-fluid phononic crystal ring resonators. Journal of Molecular Liquids, 308 (2020) 113144.

[118] Babaki J, Nazari F. Heterostructure based demultiplexer using solid-solid phononic crystal ring resonators. Journal of Physics D: Applied Physics , 53 (2020) 375301.

[119] Maldovan M, Thomas EL. Periodic Materials and Interference Lithography: for Photonics, Phononics and Mechanics. John Wiley & Sons, (2009).

[120] Morgan D. Surface acoustic wave filters: With applications to electronic communications and signal processing. Academic Press, (2010).

[121] D. P. Elford, "Band gap formation in acoustically resonant phononic crystals," Loughborough University Loughborough, Ph.D. Dissertation, (2010).

[122] Wu F, Liu Z, Liu Y. Splitting and tuning characteristics of the point defect modes in two-dimensional phononic crystals. Physical Review E, 69 (2004) 066609.

[123] Khelif A, Djafari-Rouhani B, Vasseur JO et al. Transmission and dispersion relations of perfect and defect-containing waveguide structures in phononic band gap materials. Physical Review B, 68 (2003) 024302.

[124] Khelif A, Choujaa A, Djafari-Rouhani B et al. Trapping and guiding of acoustic waves by defect modes in a full-band-gap ultrasonic crystal. Physical Review B, 68 (2003) 214301.

[125] Taleb F, Darbari S. Tunable locally resonant surface-acoustic-waveguiding behavior by acoustoelectric interaction in Zn O-based phononic crystal. Physical Review Applied, 11 (2019) 024030.
[126] Taleb F, Darbari S, Khelif A. Reconfigurable locally resonant surface acoustic demultiplexing behavior in ZnO-based phononic crystal. Journal of Applied Physics, 129 (2021) 024901.
[127] Yao ZJ, Yu GL, Wang YS et al. Propagation of bending waves in phononic crystal thin plates with a point defect. International Journal of Solids and Structures, 46 (2009) 2571-2576.
[128] Khelif A, Choujaa A, Benchabane S et al. Guiding and bending of acoustic waves in highly confined phononic crystal waveguides. Applied Physics Letter, 84 (2004) 4400-4402.
[129] Pennec Y, Djafari-Rouhani B, Vasseur JO et al. Tunable filtering and demultiplexing in phononic crystals with hollow cylinders. Physical Review E, 69 (2004) 046608.
[130] Pennec Y, Djafari-Rouhani B, Vasseur JO et al. Acoustic channel drop tunneling in a phononic crystal. Applied Physics Letter, 87 (2005) 261912.
[131] Kaya OA, Korozlu N, Trak D et al. One-dimensional surface phononic crystal ring resonator and its application in gas sensing. Applied Physics Letter, 115 (2019) 041902.
[132] Rostami-Dogolsara B, Moravvej-Farshi MK, Nazari F. Designing switchable phononic crystal-based acoustic demultiplexer. IEEE Transactions on Ultrasonics, Ferroelectrics, and Frequency Control, 63 (2016) 1468-1473.

[133] Li F, Liu J, Wu Y. The investigation of point defect modes of phononic crystal for high Q resonance. Journal of Applied Physics, 109 (2011) 124907.
[134] Cicek A, Salman A, Kaya OA et al. Sharp bends of phononic crystal surface modes. Journal of Physics: Condensed Matter, 27 (2015) 475003.
[135] Kelders L, Allard JF, Lauriks W. Ultrasonic surface waves above rectangular-groove gratings. Journal of the Acoustical Society of America, 103 (1998) 2730-2733.
[136] Zhou Y, Lu MH, Feng L et al. Acoustic Surface Evanescent Wave and its Dominant Contribution to Extraordinary Acoustic Transmission and Collimation of Sound. Physical Review Letter, 104 (2010) 164301.
[137] Jia H, Lu M, Ni X et al. Spatial separation of spoof surface acoustic waves on the graded groove grating. Journal of Applied Physics, 116 (2014) 124504.
[138] Jia H, Lu M, Wang Q et al. Subwavelength imaging through spoof surface acoustic waves on a two-dimensional structured rigid surface. Applied Physics Letter, 103 (2013) 103505.
[139] Ye Y, Ke M, Li Y et al. Liu. Focusing of spoof surface-acoustic-waves by a gradient-index structure. Journal of Applied Physics, 114 (2013) 154504.
[140] Rostami A, Kaatuzian H, Rostami-Dogolsara B. Design and analysis of tunable acoustic channel drop

filter based on fluid-fluid phononic crystal ring resonators. Wave Motion, 101 (2021) 102700.
[141] Rostami-Dogolsara B, Moravvej-Farshi MK, Nazari F. Designing phononic crystal based tunable four-channel acoustic demultiplexer. Journal of Molecular Liquids, 281 (2019) 100-107.
[142] Bahrami A, Alinejad-Naini M, Motaei F. A proposal for 1×4 phononic switch/demultiplexer using composite lattices. Solid State Communications, 326 (2021) 114179.